Photochemistry and Photobiology, 20**, **: *–*

Photodynamic Therapy in HeLa Cells Incubated with Riboflavin and Pectin-coated Silver Nanoparticles†

María Belén Rivas Aiello[1], Daniel Castrogiovanni[2], Julieta Parisi[2], Julio C. Azcárate[3], Fernando S. García Einschlag[1], Thomas Gensch[4], Gabriela N. Bosio[1,4] and Daniel O. Mártire[*1]

[1]Instituto de Investigaciones Fisicoquímicas Teóricas y Aplicadas (INIFTA), Facultad de Ciencias Exactas, Universidad Nacional de La Plata, La Plata, Argentina
[2]CCT-La Plata-CONICET, Instituto Multidisciplinario de Biologia Celular (IMBICE), La Plata, Argentina
[3]Centro Atómico Bariloche (CAB), CONICET, San Carlos de Bariloche, Río Negro, Argentina
[4]Institute of Complex Systems (ICS-4 (Cellular Biophysics)), Forschungszentrum Jülich, Jülich, Germany

Received 9 May 2018, accepted 26 June 2018, DOI: 10.1111/php.12974

ABSTRACT

Riboflavin (Rf) is an endogenous photosensitizer, which can participate in Type I and Type II processes. We have recently shown that the yield of the triplet excited states of Rf is enhanced in the presence of pectin-coated silver nanoparticles (Pec@AgNP) due to formation of a complex between Rf and Pec@AgNP (Rf-Pec@AgNP). Consequently, under aerobic conditions, the amounts of singlet molecular oxygen and superoxide radical anion generated are also larger in the presence of the nanoparticles. This result made us suspect that the nanoparticles could have a beneficial effect in Rf-based PDT. To prove this hypothesis, we here compared the photodamage in HeLa cells incubated with Rf in the presence and in the absence of Pec@AgNP applying several optical assays. We used fluorescence imaging of irradiated HeLa cells incubated with Annexin V and propidium iodide to evaluate the occurrence of apoptosis/necrosis, the reduction of the tetrazolium dye MTT to formazan and neutral red uptake to prove cell viability, as well as synchrotron infrared microscopy of single cells to evaluate possible structural changes of DNA and nuclear proteins. The enhanced photodamage observed in the presence of Pec@AgNP seems to indicate that Rf enters into the cells complexed with the nanoparticles.

INTRODUCTION

Photodynamic therapy (PDT) consists of tumor irradiation with visible or NIR light after application of a photosensitizer (1). Riboflavin (vitamin B2, Rf) is present in biological systems as a constituent of proteins binding flavin mononucleotide and flavin adenine dinucleotide as cofactors (2). Electron transfer from numerous donor molecules present in cells to the triplet state of Rf, ^{3}Rf*, yields the $RF^{\cdot-}$ radical anion, which initiates free radical reactions (Type I photosensitization) (3). In addition, upon irradiation of Rf solutions under aerobic conditions, singlet molecular oxygen, $O_2(^1\Delta_g)$, is also formed by energy transfer from ^{3}Rf* to ground state oxygen (Type II photosensitization). Consequently, the Type I and Type II photooxidation of several substrates sensitized by Rf was the topic of several publications (4,5).

The photoinduced generation of reactive oxygen species (ROS) motivated the testing of the photosensitizing ability of Rf for a number of applications. For instance, light irradiation of Rf in aqueous medium was demonstrated to be effective as antibacterial agent (6,7), as crosslinker for corneal stiffening (5,8), for blood product sterilization (9) and for the treatment of skin lesions (10).

The improved generation of $O_2(^1\Delta_g)$ by Rf in the presence of pectin-coated Ag nanoparticles (Pec@AgNP) was previously demonstrated by an indirect method (11). More recently, we have shown by time-resolved absorption spectroscopy that the decay of the excited state of the complex formed by Rf with pectin-coated Ag nanoparticles (Pec@AgNP) in aqueous solution feeds ^{3}Rf* excited state. As a result, the amounts of ^{3}Rf*, $O_2(^1\Delta_g)$, and superoxide radical anion, $O_2^{\cdot-}$, generated by Rf are enhanced in the presence of the nanoparticles (12).

There are many literature reports showing the beneficial role of heavy metals on the photodynamic activity of organic photosensitizers. In particular, several nanohybrids of organic sensitizers with noble metal nanoparticles were prepared and their performances in PDT in carcinoma cells were tested. For instance, studies performed in HeLa cells and Protoporphyrin IX with gold nanoparticles (13,14) showed a higher phototoxicity of the sensitizer when complexed with the nanomaterial. The enhanced performance of nanohybrids in PDT compared to the free sensitizers was also shown for other systems, including Au nanoparticles functionalized with zinc phthalocyanine and a lactose derivative employing SK-BR-3 breast cancer cells (15), meso-tetrahydroxy-phenylchlorin conjugated to Au nanoparticles in SH-SY5Y human neuroblastoma cells (16), pluronic-coated gold nanoparticles incorporating the hydrophobic dye IR780 in murine colon carcinoma C-26 cells (17) and gold nanocomposites with hematoporphyrin in MT-4 leukemia cells (18). In addition, *in vitro* photoactivity assays performed with a hybrid nanomaterial of Au nanoparticles decorated with Pheophorbide-A (PheoA), and the cancer-targeting agent hyaluronic acid in the lung cancer cell line (A549) showed that over 95% of the cells were dead upon laser irradiation (19). Porphyrin-decorated Au nanoparticles containing a targeting agent that recognizes the

*Corresponding author email: dmartire@inifta.unlp.edu.ar (Daniel O. Mártire)
†This article is part of a Special Issue dedicated to Dr. Norman Andi García.

erbB2 receptor overexpressed on the surface of SK-BR-3 were shown to elicit targeted PDT of these cells (20). Au nanoclusters and Chlorine 6 loaded into pH-sensitive liposomal nanocomposites were proven to be efficient nanohybrids for PDT *in vivo* (21). Examples of nanohybrids employing two-photon excitation can be found in the review article by Shen *et al.* (22).

Motivated by the enhanced generation of ROS by Rf in the presence of Pec@AgNP and by the beneficial role of metallic nanoparticles on PDT treatments, the main goal of the present work is to prove the presumable enhancing effect of Pec@AgNP on PDT when Rf is employed as a sensitizer. To this end, we here compare the photodamage induced in HeLa cells incubated with Rf in the presence and in the absence of Pec@AgNP. To evaluate the effect of PDT on the cells, we performed a series of biological assays to monitor apoptosis, necrosis, mitochondrial activity, the integrity of lysosome membrane and structural changes in DNA and nuclear proteins.

MATERIALS AND METHODS

Materials. Riboflavin, pectin from apple, furfuryl alcohol (FFA), 3-(4,5-dimethylthiazol-2-yl)-2,5-diphenyltetrazolium bromide (MTT), neutral red, Annexin V and PI were purchased from Sigma-Aldrich. Silver nitrate was obtained from Biopack and sodium hydroxide from J. T. Baker. All experiments were performed with deionized water.

Synthesis of Pec@AgNP. The reported method was employed (11).

TEM imaging. The size of Pec@AgNP was characterized by transmission electron microscopy (TEM) using a Phillips CM200-UT (LaB6) operated at 200 kV. The size of the particles was fitted with lognormal distributions.

Oxygen uptake experiments. The consumption of oxygen upon irradiation was measured with an oxygen-sensitive electrode (Consort SZ10T) in initially air-saturated solutions of Rf with and without Pec@AgNP in the presence of FFA, a well-known quencher of $O_2(^1\Delta_g)$ (23).

Cell culture. Human carcinoma HeLa cells were grown in modified Eagle's medium (MEM) (GIBCO) containing 10% FBS (Internegocios S.A.) and 100 μg mL^{-1} of penicillin. Cell cultures were performed in an incubator with 5% CO_2 and 95% air at 37°C. 1.5×10^4 cells were seeded in 96-well plates and grown for 24 h until confluence.

Cellular uptake of riboflavin. OPTIMEM media (GIBCO) were prepared with and without addition of Rf (final concentration: 50 μM). An aliquot of 1 mL volume of these media was kept in the dark for 24 h. These media will be named "before." The remaining media—containing 50 or 0 μM—were employed for the incubation of HeLa cells for 24 h. Then, cells were counted and the fluorescence (λ^{exc} = 488 nm, λ^{em} = 530 nm) of every sample was measured (before and after cell growth) and corrected by the number of cells.

Cytotoxicity assay in dark. HeLa cells (1.5×10^4) were plated in 100 μL MEM (GIBCO) containing 10% FBS (Internegocios S.A.) and 100 μg mL^{-1} of penicillin, and incubated overnight at 37°C with 5% CO_2 until confluence. The medium was then removed and the cells were incubated for 24 h with different concentrations of Rf, Pec@AgNP or a mixture in MEM. Every experiment was compared to a control culture. Cell survival was assessed by MTT and NRU assay as described previously (24–26).

PDT phototoxicity assay. The procedure was the same as in the dark assay. After de incubation with Riboflavin, Pec@AgNP or the mixture, the medium was changed for DMEM/F12 (GIBCO) without phenol red and the samples were irradiated with two RPR-3500 A lamp with emission centered at 350 nm for 2 h into the cell incubator. The emission spectrum of the lamp is shown in Figure S1 (see Supporting Information). The irradiance measured using potassium ferrioxalate as actinometer (27) with the same irradiation geometry was 9.6 mW cm^{-2}. Photocytotoxicity was evaluated by MTT and NRU assay (28,29).

Annexin V/propidium iodide (PI) staining assay evaluated by fluorescence microscopy. HeLa cells exposed to Pec@AgNP in the presence as well in the absence of Rf, or to Rf alone and without any additives were cultivated as indicated above into a glass bottom 35 mm Petri dish (ibidi, Martinsried, Germany), previously treated with Poly-L-Lysine (PLL) (0.1 mg mL^{-1}) (1 mL for 5 min). After 24 h of incubation, the cell culture was washed twice with PBS buffer of pH 7.4. Samples were then placed directly inside a stage top incubator (Okolab S.R.L., Pozzuoli, Italy; environmental parameters set to 37°C, 85% humidity and 5% CO_2) on the stage of an inverted microscope (Ti-E, Nikon) and 1 mL of Binding Buffer BD Pharmingen was added. The inverted microscope was used as a spinning disk confocal microscope (30) (ACALBFI, Groeben, Germany) with a spinning disk unit (CSU-W1; Yokogawa Electric Corporation, Tokyo, Japan) as the central part, and an EMCCD camera (Ixon Ultra 897; Andor Technologies Ltd., Belfast, UK) as a detector and an image splitting device (Optosplit II; Cairn Research, Faversham, UK) for simultaneous observation of two spectral regions of the emitted light (with the option of using one or two simultaneous excitation light sources). Bright field images, as well as spinning disk confocal fluorescence images with excitation at 488 and 561 nm, were taken with a 100× magnification immersion objective (plan apo chromat, NA = 1.40, Nikon). Appropriate dichroic beam splitter and bandpath filters in the Optosplit unit allowed the simultaneous detection of fluorescence in two spectral regions, 500–550 nm (Annexin V-FITC excited by 488 nm laser) and 590–650 nm (PI excited by 561 nm laser), respectively. The software Andor IQ2 was used for image acquisition. Exposure time for single image was set 200 ms and the frame rate was set the minimal. Irradiation for photodynamic action: HeLa cells were then illuminated with a 405 nm laser (417 mW cm^{-2}), for 5 min to induce photodamage. Afterward, 1 mL Annexin V/PI solution (50 μL Annexin V-FITC—BD Pharmingen 10× +20 μL PI 50 μg mL^{-1} BD Pharmingen + 930 μL Binding Buffer) was carefully added without moving the sample. After 15 min of incubation in the dark, both PI fluorescence (excitation at 561 nm (116 mW cm^{-2}, 200 ms), emission maximum at 620 nm) and Annexin V-FITC fluorescence (excitation at 488 nm (60.9 mW cm^{-2}, 200 ms), emission maximum at 530 nm) images were recorded. Control experiments were performed in HeLa cells without nanoparticles but with Rf and without neither of the two.

FTIR microspectroscopy. The experiments were performed at the infrared SMIS beamline (SOLEIL Synchrotron, L'Orme des Merisiers, Gif sur Yvette, France). The synchrotron-based Fourier transform infrared (SR-FTIR) microspectroscopy was employed to investigate structural changes of DNA and nuclear proteins of HeLa cells grown on CaF_2 slides. Spectra were taken specifically on the cells nuclei in transmission mode. The instrumentation, methods and conditions used have been previously described (31). Cell spectra recorded one by one, with 50–100 individual cells per sample were analyzed. Principal component analysis (PCA) was used for outliers detection within samples and also for comparison between samples. The preprocessing methods of the spectra have been described elsewhere (31). Briefly, the Savitzky–Golay algorithm was applied either to perform a baseline correction of the raw data (zero order spectra) or to evaluate the second derivative of the data (second order spectra) (31). Before executing PCA routines, the spectra obtained by the latter procedures were scaled to unit norm within the desired wave number range.

RESULTS

TEM images of Pec@AgNP

We have prepared pectin-coated silver nanoparticles according to the reported procedure (12). A typical TEM image and its corresponding histogram are shown in Fig. 1. The measured nanoparticles size can be described by a bimodal distribution with an average of 2.3 ± 0.7 nm (major fraction; >95%) and 9 ± 6 nm.

Effect of Pec@AgNP in oxygen uptake

From now on, the concentration of Ag will be specified instead of that of Pec@AgNP. Note that from the average diameter of the spherical nanoparticles (2.3 nm) and neglecting the contribution of the bigger particles, an average volume of the nanoparticles of 6.37×10^{-21} cm^3 is obtained. Taking the reported metal

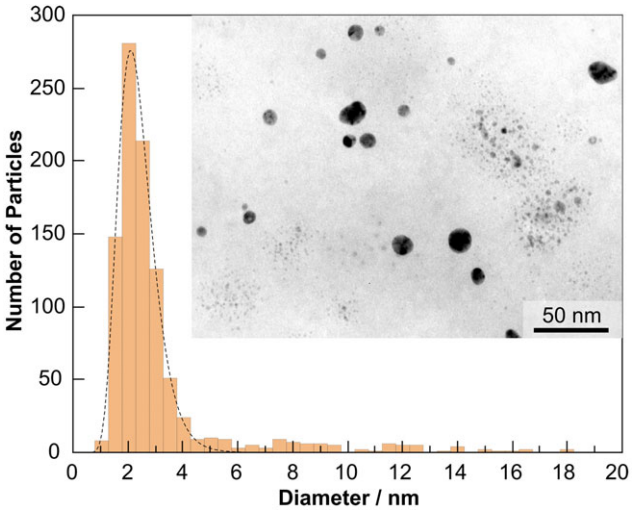

Figure 1. Transmission electron microscopy (TEM) bright field image of Pec@AgNP and the size distribution histogram of 956 particles.

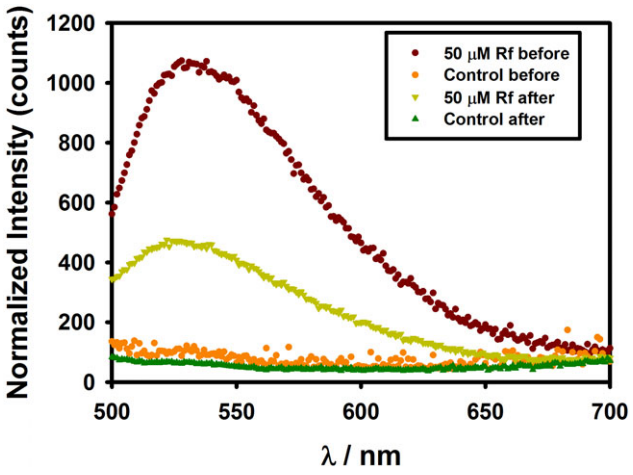

Figure 2. Emission spectra (λ^{exc} = 488 nm) of Rf in OPTIMEM medium before and after incorporation into HeLa cells, as indicated. The emission of the control media without Rf before and after incubation is also shown.

density of 10.5 g cm^{-3} (32), the molar concentration of the nanoparticles results 3.73 × 10^2 times lower than that of Ag.

Oxygen uptake experiments with samples containing FFA were performed. The results are shown in Figure S2 of the Supporting Material. The rate of oxygen uptake is slightly enhanced by the presence of Pec@AgNP ([Ag] = 1 μM), which is within the concentration range used in the biological assays. This result is in line with the increase of $O_2(^1\Delta_g)$ yield produced by Rf in the presence of Pec@AgNP, which was previously demonstrated in time-resolved phosphorescence experiments. According to the phosphorescence assays, a larger increment in rate of oxygen uptake is expected for concentrations of Pec@AgNP higher than those employed in the present work (12).

Cellular uptake of riboflavin

The uptake of Rf in HeLa cells was measured by fluorescence. Comparison of the fluorescence emission spectra (λ^{exc} = 488 nm) of the Rf solutions before and after incorporation of the dye in the cells is shown in Fig. 2. We tested different Rf concentrations and the uptake was always significant and in the range of 50%, as shown here for OPTIMEM medium containing 50 μM Rf.

MTT and NRU tests

Two different tests for cyto/phototoxicity were employed: 3-(4,5-dimethylthiazol-2-yl)-2,5-diphenyltetrazolium bromide (MTT) reactivity and neutral red uptake (NRU). The former assay determines mitochondrial dehydrogenase activities in living cells. In metabolic active cells, MTT is reduced to formazan crystals by nicotinamide adenine dinucleotide hydride (NADH). The purple crystals of formazan extracted from lysed cells are then dissolved in an organic solvent and the absorbance is measured at 570 nm (33). The NRU test is based on the ability of viable cells to incorporate and enrich the dye in lysosomes via the endocytotic route. After extraction of the dye with an acidified ethanol solution, its concentration is determined spectrophotometrically (24).

3-(4,5-dimethylthiazol-2-yl)-2,5-diphenyltetrazolium bromide and NRU assays performed with nonirradiated HeLa cells incubated with Rf in the concentration range from 0 to 100 μM or Pec@AgNP containing silver in the concentration range from 0 to 1 μM delivered no evidence that, under our experimental conditions, Rf or the Pec@AgNP have an inherent adverse effect on HeLa cells (see Figure S3). Similar results were obtained with cells incubated with Rf (50 μM) and different amounts of the nanoparticles (Fig. 3D).

Assays performed with irradiated HeLa cells showed that increasing the concentration of Rf in the medium from 0 to 25 μM has no effect on the cell's ability to reduce MTT to formazan. At higher Rf concentrations (25–100 μM), a decrease in the cell's viability compared to that of the control is observed (Fig. 3A). NRU assays, which test the dye uptake by active cells and its incorporation into lysosomes, showed a decrease in the number of viable cells for Rf concentrations equal or larger than 25 μM (Fig. 3A).

The presence of Pec@AgNP ([Ag] in the range from 0.25 to 1 μM) in the preincubation medium of irradiated HeLa cells has no effect on the ability of the cells to reduce MTT to formazan nor on the incorporation of neutral red to lysosomes (Fig. 3B).

To check the possible enhanced photodamage caused by the nanoparticles in the presence of Rf, MTT and NRU assays were performed with cells incubated with Rf (50 μM) and different amounts of Pec@AgNP ([Ag] ranging from 0.25 to 1 μM). The addition of the nanoparticles produced a further decrease in cell's viability as sensed by MTT, but not by the NRU assay (Fig. 3C).

Annexin V/PI tests

It is accepted that apoptosis is the main mechanism of cell death when cells are treated with PDT *in vitro* (34). In particular, it was shown that irradiation of HL-60 and murine NS0/2 tumor cells in a culture medium enriched with Rf induces cell death by apoptosis (35,36). On the basis of these results, we performed here Annexin V/propidium iodide (PI) tests with fluorescence detection with HeLa cells previously incubated with Rf with and

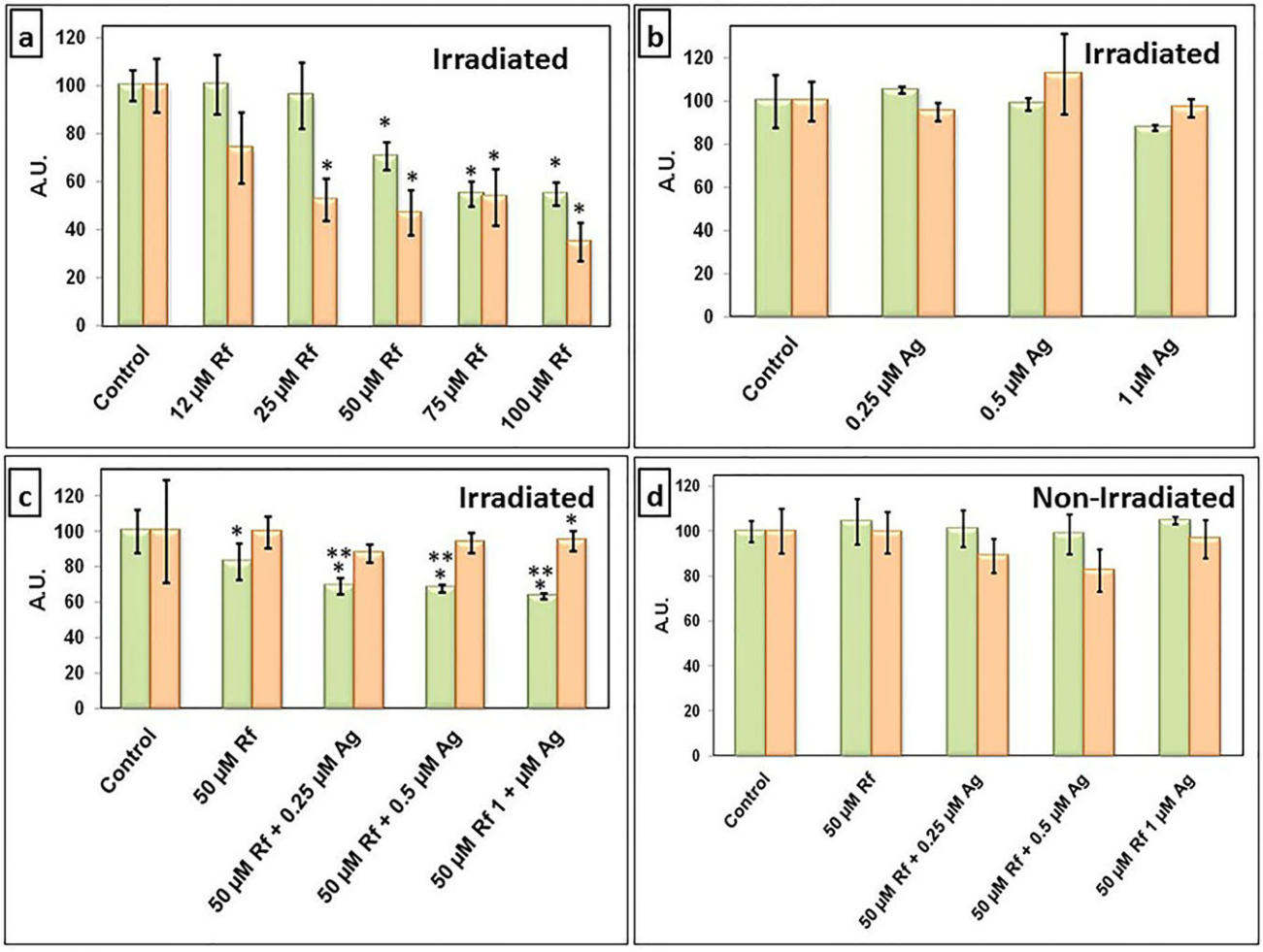

Figure 3. Histograms showing the results of the MTT (green) and neutral red uptake (NRU) (orange) assays on irradiated (A,B,C) and nonirradiated (D) HeLa cells. Values of formazan and neutral red absorbance were normalized against average values obtained from the control (irradiated cells to which neither Rf nor Pec@AgNP had not been added). The data shown were obtained from experiments in which Rf (A), Pec@AgNP (B) and Rf + Pec@AgNP (C,D) were present in the incubation medium. Error bars refer to one standard deviation; in each case, the number of samples examined was at least 4 and as large as 8. The asterisk indicates that there is a statistically significant difference between this particular number and the number obtained from the control. The double asterisk means a statistically significant difference from the irradiated sample with Rf (one-way ANOVA with Fisher's post hoc test; $P < 0.05$).

without Pec@AgNP. Annexin V reveals the presence of phosphatidylserine on the cell surface, which is indicative of an early stage of apoptosis. On the other hand, PI is used as a marker of membrane disintegrity and necrosis (37,38).

Irradiated HeLa cells preincubated with 50 μM Rf yielded a positive result to Annexin V, but negative to PI (see Fig. 4) indicating early apoptosis. In contrast, when Pec@AgNP were additionally included in the culture medium, not only Annexin V but also PI yielded positive results, thus indicating late apoptosis or necrosis. These results show a higher photodamage achieved in the presence of Pec@AgNP and Rf.

SR-FTIR microspectroscopy

Synchrotron-based Fourier transform infrared (SR-FTIR) microspectroscopy was used to detect any intracellular biochemical modification following the photoirradiation of HeLa cells containing Rf and/or the nanoparticles. Comparative assays with cells incubated with the sensitizer 5,10,15,20-Tetrakis (1-methyl-4-pyridinio) porphyrin tetra (p-toluenesulfonate), TMPyP, were performed. The visible light irradiation conditions were similar to those previously employed to show changes in the protein secondary structures in cells incubated with TMPyP (31).

Recorded FTIR data were preprocessed to yield zero order and second order spectra. PCA scores, the corresponding scree plots and sample mean zero order spectra in the region of the Amide I and Amide II bands (1480–1720 cm^{-1}), are shown in Fig. 5 for nonirradiated and irradiated HeLa cells without the addition of Rf or Pec@AgNP in the incubation medium (controls), irradiated HeLa cells preincubated with 50 μM Rf, irradiated HeLa cells preincubated with 1 μM Ag, irradiated HeLa cells preincubated with 50 μM Rf and 1 μM Ag, and irradiated HeLa cells preincubated with 10 μM TMyP for comparison.

PC1 (explaining 87% of the variation) seemed to distinguish between PDT-treated HeLa cells employing TMPyP as the sensitizer from all the other samples (31). Irradiation of HeLa cells incubated with TMPyP, which tends to accumulate in the cell nucleus, was reported to induce pronounced changes in the

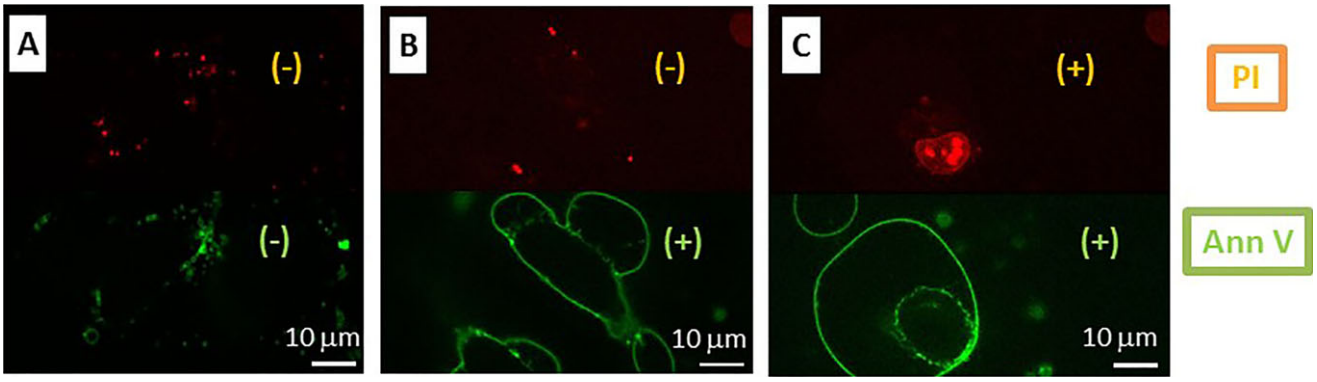

Figure 4. Fluorescence images taken after 405 nm (142 μW) irradiation for 5 min. The excitation wavelength was 561 nm (40 μW) and the maximum emission wavelength was 620 nm for PI test. For the Annexin V-FITC (AnnV) fluorescence, the excitation was at 488 nm (21 μW), and the maximum emission wavelength was 530 nm. (A) Control (B) 50 μM of Rf (C) 50 μM of Rf and 1 μM of Ag.

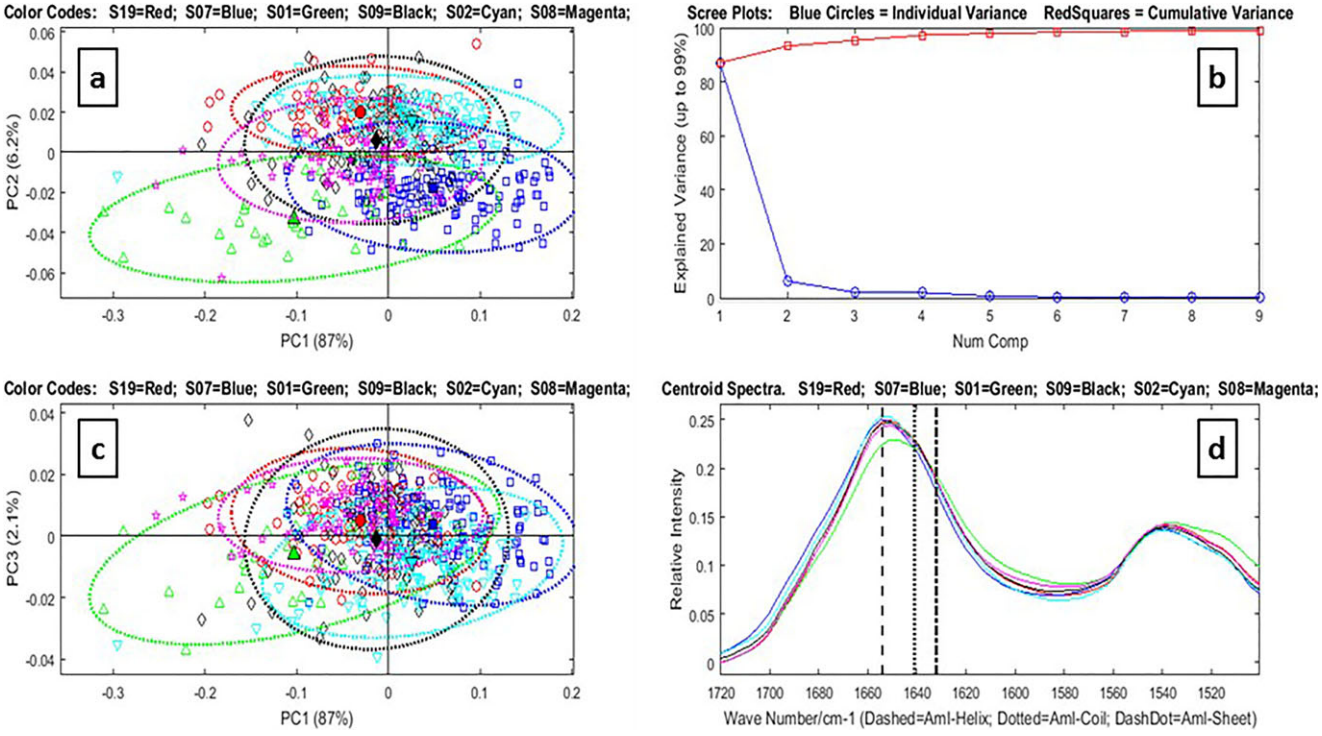

Figure 5. PCA scores: PC2 *vs* PC1 (A), PC3 *vs* PC1 (C), scree plot (B) and sample mean of zero order spectra (D) in the region of the Amide I and Amide II bands (1480–1720 cm^{-1}) of the following samples: nonirradiated (blue) and irradiated (red) HeLa cells without the addition of Rf or Pec@AgNP in the incubation medium (controls); irradiated HeLa cells preincubated with 50 μM Rf (magenta), irradiated HeLa cells preincubated with 1 μM Ag (black), irradiated HeLa cells preincubated with 50 μM Rf and 1 μM Ag (cyan), and irradiated HeLa cells preincubated with 10 μM TMyP for comparison (green). Vertical lines show the wavenumbers expected for the peaks of α-helix (1654 cm^{-1}), β-sheet (1632 cm^{-1}) and unordered random coil (1641 cm^{-1}) (26,41).

structure in the Amide I band (decrease in the portion of α-helix) (31).

These results indicate that it was not possible to detect by SR-FTIR microspectroscopy any significant change in the secondary structure of nuclear proteins of irradiated HeLa cells preincubated with Rf and/or Pec@AgNP. Similar results were obtained after submission of the spectra to different pretreatments (see the analysis of the derivative of the spectra in Figure S4). To inspect any change in the region of the Amide III peak and also include the absorption of nucleic acids, the PCA analysis was also performed in an extended wavenumber region (1748–952 cm^{-1}) (39). In this region, independent of the data pretreatment employed it was also observed that only the sample incubated with TMPyP showed a different behavior, confirming that under the conditions of our experiments, only the use of the porphyrin as photosensitizer affected the IR absorption of the protein amides of the proteins as well as nucleic acids (see Figures S5 and S6).

Although SR-FTIR spectra of HeLa cells preincubated with Rf show no changes after PDT treatment, MTT and NRU assays

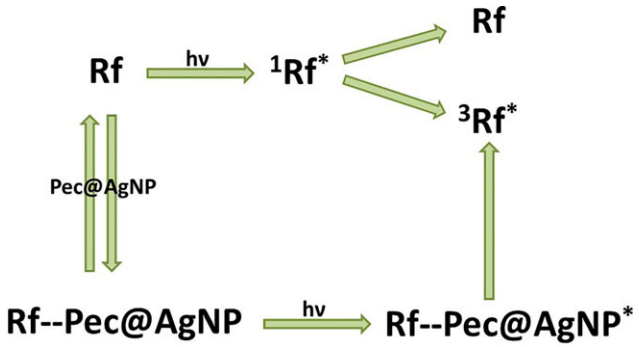

Scheme 1. Effect of Pec@Ag on the generation of the triplet excited state of Rf (^{3}Rf*). Here Rf and ^{1}Rf* represent the ground-state and electronic excited singlet state of the dye, respectively. Rf- -Pec@AgNP and Rf- -Pec@AgNP* represent the ground-state and excited state of the complex between Rf and Pec@AgNP.

evidenced lower viability of irradiated cells. The MTT test also indicated a decreased viability when the nanoparticles were added along with Rf to the incubation medium. However, we should consider that the MTT assays reflect the mitochondrial activity, NRU the lysosomal activity, whereas SR-FTIR microspectroscopy analyzes global structural changes of the biological molecules in the cells nuclei. Under the conditions of our experiments, these latter alterations were in fact detected when TMPyP was used as the sensitizer, but not with Rf. This could be related to the different localization of TMPyP and Rf. The porphyrin accumulates in the cell nucleus (31), whereas endocytic compartments are involved in the uptake and intracellular trafficking of Rf (40).

DISCUSSION

In this paper, we proved that incubation of HeLa cells with normal cell medium containing additionally Rf and Pec@AgNP lead to the incorporation of both the dye and the nanomaterial. We have previously demonstrated that a 1:1 complex (Rf-Pec@AgNP) between Rf and Pec@AgNP is formed (12). While it is not possible for us to determine directly, that is, by spectroscopic means, whether and to which extent the complex exists, when incorporated into the cells, we have here given evidence for the synergistic photodamage effect by the nanoparticles and Rf (see Figs. 3 and 4). This is interpreted as a consequence of the presence of Rf and Pec@AgNP in the same intracellular microenvironment. According to a previous publication of our laboratory, the enhancement of the amount of ROS ($O_2(^1\Delta_g)$ and $O_2^{\cdot-}$) generated by Rf in the presence of Pec@AgNP is a consequence of the decay of the excited state of the complex Rf-Pec@AgNP*, which feeds the triplet state of Rf (^{3}Rf*) (12) (Scheme 1). Thus, we here propose that the uptake of the complex is the responsible for the increased photodamage effect observed when Pec@AgNP and Rf are present (see MTT in Fig. 3 and Annexin V/PI in Fig. 4).

In summary, our results clearly show the beneficial role of Pec@AgNP on the photodynamic activity of Rf in mammalian cells. Given the nature of Rf, which is a natural vitamin able to cross biological membranes, the phototreatment proposed here looks promising for many other biological applications.

Acknowledgements—This manuscript is part of a collection of articles to honor the work of our colleague and friend Norman A. García (Andi), who actively contributed in the past 40 years to the development of basic and applied photochemistry. We acknowledge SOLEIL for provision of synchrotron radiation facilities and we would like to thank Christophe Sandt for assistance in using "SMIS" beamline. This work has been supported by grants PICT 2012-1817 and PICT 2016-0974 from ANPCyT, Argentina, and by Proposal 20160848 on SMIS beamline from SOLEIL. G.N.B.'s work in the laboratory of T.G. was financed by a grant from the Federal Ministry of Education and Research (OptoSys, FKZ 031A16) of the Federal Republic of Germany. M.B.R.A. thanks CONICET for a graduate studentship. G.N.B., J.C.A. and F.S.G.E. are permanent research staff of CONICET, Argentina. D.O.M. is permanent research staff of CIC, Buenos Aires, Argentina.

SUPPORTING INFORMATION

Additional supporting information may be found online in the Supporting Information section at the end of the article:

Figure S1. Emission spectrum of the 8 RPR-3500 A lamps with emission centered at 350 nm.

Figure S2. Oxygen uptake experiments with samples containing 54 μM Rf and 10 mM FFA: Without Nanoparticles (brown dots), with 0.5 μM of Ag (orange dots) and with 1 μM of Ag (green dots).

Figure S3. Histograms showing the results of the MTT (green) and NRU (orange) assays on nonirradiated HeLa cells treated with different concentrations of Ag (A) or Rf (B) in the incubation medium.

Figure S4. PCA scores: PC2 *vs* PC1 (upper left panel), PC3 *vs* PC1 (lower left panel), scree plot (upper right panel) and sample mean of second order derivative spectra (lower right panel) in the region of the Amide I and Amide II bands (1480–1720 cm^{-1}) of the following samples: nonirradiated (blue) and irradiated (red) HeLa cells without the addition of Rf or NPs in the incubation medium (controls); irradiated HeLa cells preincubated with 50 μM Rf (magenta), irradiated HeLa cells preincubated with 1 μM M Ag (black), irradiated HeLa cells preincubated with 50 μM Rf and 1 μM Ag (cyan), and irradiated HeLa cells preincubated with 10 μM TMyP for comparison (green). Vertical lines show the wavenumbers expected for the peaks of α-helix (1654 cm^{-1}), β-sheet (1632 cm^{-1}), and unordered random coil (1641 cm^{-1}).

Figure S5. PCA scores: PC2 *vs* PC1 (upper left panel), PC3 *vs* PC1 (lower left panel), scree plot (upper right panel) and sample mean of zero order spectra (lower right panel) in the region of the Amide I and Amide II bands (1480–1720 cm^{-1}) of the following samples: nonirradiated (blue) and irradiated (red) HeLa cells without the addition of Rf or NPs in the incubation medium (controls); irradiated HeLa cells preincubated with 50 μM Rf (magenta), irradiated HeLa cells preincubated with 1 μM M Ag (black), irradiated HeLa cells preincubated with 50 μM Rf and 1 μM Ag (cyan), and irradiated HeLa cells preincubated with 10 μM TMyP for comparison (green). Vertical lines show the wavenumbers expected for the peaks of α-helix (1654 cm^{-1}), β-sheet (1632 cm^{-1}), and unordered random coil (1641 cm^{-1}).

Figure S6. PCA scores: PC2 *vs* PC1 (upper left panel), PC3 *vs* PC1 (lower left panel), scree plot (upper right panel) and sample mean of second order derivative spectra (lower right panel)

in the region of the Amide I and Amide II bands (1480–1720 cm^{-1}) of the following samples: nonirradiated (blue) and irradiated (red) HeLa cells without the addition of Rf or NPs in the incubation medium (controls); irradiated HeLa cells preincubated with 50 μM Rf (magenta), irradiated HeLa cells preincubated with 1 μM M Ag (black), irradiated HeLa cells preincubated with 50 μM Rf and 1 μM Ag (cyan), and irradiated HeLa cells preincubated with 10 μM TMyP for comparison (green). Vertical lines show the wavenumbers expected for the peaks of α-helix (1654 cm^{-1}), β-sheet (1632 cm^{-1}), and unordered random coil (1641 cm^{-1}).

REFERENCES

1. Juarranz, Á., P. Jaén, F. Sanz-Rodríguez, J. Cuevas and S. González (2008) Photodynamic therapy of cancer. Basic principles and applications. *Clin. Transl. Oncol.* **10**, 148–154.
2. Cardoso, D. R., S. H. Libardi and L. H. Skibsted (2012) Riboflavin as a photosensitizer. Effects on human health and food quality. *Food Funct.* **3**, 487–502.
3. Escalada, J. P., A. Pajares, J. Gianottia, A. Biasuttib, S. Criado, P. Molinab, W. Massad, F. Amat-Guerric and N. A. García (2011) Photosensitized degradation in water of the phenolic pesticides bromoxynil and dichlorophen in the presence of riboflavin, as a model of their natural photodecomposition in the environment. *J. Hazard. Mater.* **186**, 466–472.
4. Montaña, M. P., W. A. Massad, S. Criado, A. Biasutti and N. A. García (2010) Stability of flavonoids in the presence of riboflavin-photogenerated reactive oxygen species: a kinetic and mechanistic study on quercetin, morin and rutin. *Photochem. Photobiol.* **86**, 827–834.
5. Challier, C., D. O. Mártire, N. A. García and S. Criado (2017) Visible light-mediated photodegradation of imidazoline drugs in the presence of Riboflavin: possible undesired effects on imidazoline-based eye drops. *J. Photochem. Photobiol. A Chem.* **332**, 399–405.
6. Halili, F., A. Arboleda, H. Durkee, M. Taneja, D. Miller, K. A. Alawa, M. C. Aguilar, G. Amescua, H. W. Jr Flynn and J. M. Parel (2016) Rose Bengal- and riboflavin-mediated photodynamic therapy to inhibit methicillin-resistant *Staphylococcus aureus* keratitis isolates. *Am. J. Ophthalmol.* **166**, 194–202.
7. Thakuri, P. S., R. Joshi, S. Basnet, S. Pandey, S. D. Taujale and N. Mishra (2011) Antibacterial photodynamic therapy on *Staphylococcus aureus* and *Pseudomonas aeruginosa* in-vitro. *Nepal Med. Coll. J.* **13**, 281–284.
8. Chan, T. C., T. W. Lau, J. W. Lee, I. Y. Wong, V. Jhanji and R. L. Wong (2015) Corneal collagen cross-linking for infectious keratitis: an update of clinical studies. *Acta Ophthalmol.* **93**, 689–696.
9. Ettinger, A., M. M. Miklauz, D. J. Bihm, G. Maldonado-Codina and R. P. Goodrich (2012) Preparation of cryoprecipitate from riboflavin and UV light-treated plasma. *Transfus. Apher. Sci.* **46**, 153–158.
10. Sato, K., N. Sakakibara, K. Hasegawa, H. Minami and T. Tsuji (2000) A preliminary report of the treatment of blue nevus with dermal injection of riboflavin and exposure to near-ultraviolet/visible radiation (ribophototherapy). *J. Dermatol. Sci.* **23**, 22–26.
11. De Melo, L. S. A., A. S. L. Gomes, S. Saska, K. Nigoghossian, Y. Messaddeq, S. J. L. Ribeiro and R. E. De Araujo (2012) Singlet oxygen generation enhanced by silver-pectin nanoparticles. *J. Fluoresc.* **22**, 1633–1638.
12. Rivas Aiello, M. B., J. J. Romero, S. G. Bertolotti, M. C. Gonzalez and D. O. Mártire (2016) Effect of silver nanoparticles on the photophysics of riboflavin: consequences on the ROS generation. *J. Phys. Chem. C* **120**, 21967–21975.
13. Savarimuthu, W. P., P. Gananathan, A. P. Rao, E. Manickam and G. Singaravelu (2015) Protoporphyrin IX-gold nanoparticle conjugates for targeted photodynamic therapy–an in-vitro study. *J. Nanosci. Nanotechnol.* **15**, 5577–5584.
14. Eshghi, H., A. Sazgarnia, M. Rahimizadeh, N. Attaran, M. Bakavoli and S. Soudmand (2013) Protoporphyrin IX-gold nanoparticle conjugates as an efficient photosensitizer in cervical cancer therapy. *Photodiagnosis Photodyn. Ther.* **10**, 304–312.
15. García Calavia, P., I. Chambrier, M. J. Cook, A. H. Haines, R. A. Field and D. A. Russell (2018) Targeted photodynamic therapy of breast cancer cells using lactose-phthalocyanine functionalized gold nanoparticles. *J. Colloid Interface Sci.* **512**, 249–259.
16. Haimov, E., H. Weitman, S. Polani, H. Schori, D. Zitoun and O. Shefi (2018) mTHPC- conjugated gold nanoparticles as a tool to improve photodynamic therapy. *ACS Appl. Mater. Interfaces.* **10**, 2319–2327.
17. Nagy-simon, T., M. Potara, A. Craciun, E. Licarete and S. Astilean (2018) Journal of Colloid and Interface Science IR780-dye loaded gold nanoparticles as new near infrared activatable nanotheranostic agents for simultaneous photodynamic and photothermal therapy and intracellular tracking by surface enhanced resonant Raman scattering imaging. *J. Colloid Interface Sci.* **517**, 239–250.
18. Gamaleia, N. F., E. D. Shishko, G. A. Dolinsky, A. B. Shcherbakov, A. V. Usatenko and V. V. Kholin (2010) Photodynamic activity of hematoporphyrin conjugates with gold nanoparticles: experiments *in vitro*. *Exp. Oncol.* **32**, 44–47.
19. Kang, S. H., M. Nafiujjaman, M. Nurunnabi, H. A. Li Li, K. J. Khan, K M Huh Cho and Y. Lee (2015) Hybrid photoactive nanomaterial composed of gold nanoparticles, pheophorbide-A and hyaluronic acid as a targeted bimodal phototherapy. *Macromol. Res.* **23**, 474–484.
20. Penon, O., M. J. Marín, D. A. Russell and L. Pérez-García (2017) Water soluble, multifunctional antibody-porphyrin gold nanoparticles for targeted photodynamic therapy. *J. Colloid Interface Sci.* **496**, 100–110.
21. Gao, F., W. Zheng, L. Gao, P. Cai, R. Liu, Y. Wang, Q. Yuan, Y. Zhao and X. Gao (2017) Au nanoclusters and photosensitizer dual loaded spatiotemporal controllable liposomal nanocomposites enhance tumor photodynamic therapy effect by inhibiting thioredoxin reductase. *Adv. Healthc. Mater.* **6**, 1601453.
22. Chen, J., Z. Sheng, P. Li, M. Wu, N. Zhang, X. Yu, Y. Wang, D. Hu, H. Zheng and G. P. Wang (2017) Indocyanine green-loaded gold nanostars for sensitive SERS imaging and subcellular monitoring of photothermal therapy. *Nanoscale* **44**, 234–239.
23. Bosio, G. N., P. David Gara, F. S. Einschlag, M. C. Gonzalez, M. T. Del Panno and D. O. Mártire (2008) Photodegradation of soil organic matter and its effect on gram-negative bacterial growth. *Photochem. Photobiol.* **84**, 1126–1132.
24. Repetto, G., A. del Peso and J. L. Zurita (2008) Neutral red uptake assay for the estimation of cell viability/cytotoxicity. *Nat. Protoc.* **3**, 1125–1131.
25. Bosio, G. N., T. Breitenbach, J. Parisi, M. Reigosa, F. H. Blaikie, B. W. Pedersen, E. F. F. Silva, D. O. Mártire and P. R. Ogilby (2013) Antioxidant β-carotene does not quench singlet oxygen in mammalian cells. *J. Am. Chem. Soc.* **135**, 272–279.
26. Stockert, J. C., R. W. Horobin, L. L. Colombo and A. Blázquez-Castro (2018) Tetrazolium salts and formazan products in Cell Biology: viability assessment, fluorescence imaging, and labeling perspectives. *Acta Histochem.* **120**, 159–167.
27. Quan, Y., S. O. Pehkonen and M. B. Ray (2004) Evaluation of three different lamp emission models using novel application of potassium ferrioxalate actinometry. *Ind. Eng. Chem. Res.* **43**, 948–955.
28. Twentyman, P. R. and M. Luscombe (1987) A study of some variables in a tetrazolium dye (MTT) based assay for cell growth and chemosensitivity. *Br. J. Cancer* **56**, 279–285.
29. Mosmann, T. (1983) Rapid colorimetric assay for cellular growth and survival: application to proliferation and cytotoxicity assays. *J. Immunol. Methods* **65**, 55–63.
30. Oreopoulos, J., R. Berman and M. Browne (2014) Chapter 9 – Spinning-disk confocal microscopy: present technology and future trends. *Methods Cell Biol.* **123**, 153–175.
31. Bosio, G. N., J. Parisi, F. S. García Einschlag and D. O. Mártire (2018) Imidazole and beta-carotene photoprotection against photodynamic therapy evaluated by synchrotron infrared microscopy. *Spectrochim. Acta A Mol. Biomol. Spectrosc.* **195**, 53–61.
32. Liu, X., M. Atwater, J. Wang and Q. Huo (2007) Extinction coefficient of gold nanoparticles with different sizes and different capping ligands. *Colloids Surf. B Biointerfaces* **58**, 3–7.
33. Li, W., J. Zhou and Y. Xu (2015) Study of the in-vitro cytotoxicity testing of medical devices (Review). *Biomed. Rep.* **3**, 617–620.

34. Abrahamse, H. and M. R. Hamblin (2016) New photosensitizers for photodynamic therapy. *Biochemistry* **473**, 347–364.
35. Edwards, A. M., E. Silva, B. Jofré, M. I. Becker and A. E. De Ioannes (1994) Visible light effects on tumoral cells in a culture medium enriched with tryptophan and riboflavin. *J. Photochem. Photobiol., B* **24**, 179–186.
36. Edwards, A. M., F. Barredo, E. Silva, A. E. De Ioannes and M. I. Becker (1999) Apoptosis induction in nonirradiated human HL-60 and murine NSO/2 tumor cells by photoproducts of indole-3-acetic acid and riboflavin. *Photochem. Photobiol.* **70**, 645–649.
37. Yang, Y., Y. Xiang and M. Xu (2015) From red to green: the propidium iodide-permeable membrane of Shewanella decolorationis S12 is repairable. *Sci. Rep.* **5**, 2–6.
38. Rieger, A. M., K. L. Nelson, J. D. Konowalchuk and D. R. Barreda (2011) Modified Annexin V/propidium iodide apoptosis assay for accurate assessment of cell death. *J. Vis. Exp.* **50**, 3–6.
39. Gasparri, F. and M. Muzio (2003) Monitoring of apoptosis of HL60 cells by Fourier-transform infrared spectroscopy. *Biochem. J.* **248**, 239–248.
40. Huang, S. N., M. Phelps and P. W. Swaan (2003) Involvement of endocytic organelles in the subcellular trafficking and localization of riboflavin. *J. Pharmacol. Exp. Ther.* **306**, 681–687.
41. André, W., C. Sandt, P. Dumas, P. Djian and G. Hoffner (2013) Structure of inclusions of Huntington's disease brain revealed by synchrotron infrared microspectroscopy: polymorphism and relevance to cytotoxicity. *Anal. Chem.* **85**, 3765–3773.